Transient Response Characteristics Improvement of Permanent Magnet Synchronous Motor Based on Enhanced Linear Active Disturbance Rejection Sensorless Control

Yao Xu, *Student Member, IEEE*, Cheng Lin, and Jilei Xing

***Abstract*—The compactness, cost decrease, and reliability of the auxiliary drive permanent magnet synchronous motors (PMSMs) for battery electric commercial vehicles can be further improved by adopting the position sensorless control technique. The conventional extended back electromotive force (EEMF) based sensorless control algorithm usually requires a phase-locked loop (PLL) and low pass filter to postprocess the estimated rotor position, which deteriorates the transient response of the PMSM significantly. To solve this problem, this article proposes an active disturbance rejection control based EEMF sensorless control method. By designing an extended state observer (ESO) considering the differential term of the position estimation error, timely and accurate estimation of the load disturbance and rotor position can be achieved simultaneously. The adaptive mechanism of the ESO exhibits sound system antidisturbance performance. Moreover, a linear state error feedback controller and feedforward compensation of load disturbance can replace the speed loop PI controller accordingly. Through stability and tracking performance analysis, the proposed method is superior in both steady-state performance and transient-state performance. The proposed scheme is experimentally validated by a 3 kW automotive power steering oil pump motor drive system. The results show that the transient response characteristics are obviously enhanced compared with the conventional methods.[1]**

***Index Terms*—Bandwidth adaptive mechanism, extended back electromotive force (EEMF) estimation, enhanced linear active disturbance rejection control (ELADRC), Permanent magnet synchronous motor (PMSM), sensorless control.**

I. Introduction

PERMANENT magnet synchronous motors (PMSMs) are being widely employed to drive power steering oil pumps and electric brake air pumps for battery electric commercial vehicles on account of the advantages of high efficiency and high power density [1], [2], [3], [4], [5], which are usually referred to as auxiliary drive motors (ADMs) under such conditions. Due to installation space constraints and cost-saving considerations, rotor position sensors in ADMs are being phased out. Toward this end, sensorless control has been widely and intensively researched by academia and industry in the last decade conducive to improving the reliability and stability of the control system of PMSM.

Depending on the scope of the motor speed, there are different classifications of sensorless control methods for PMSM [6], [7], [8]. In the medium- and high-speed operation regions, methods based on motor mathematical models, such as the back electromotive force (BEMF) estimation method [9], [10], are applied regularly. However, in the zero- and low-speed operation regions, the model authenticity is strongly influenced by the motor parameters, and the rotor position estimation accuracy of these methods decreases sharply. Therefore, methods based on the saliency, such as the high-frequency (HF) signal injection method [11], [12], are more suitable for these operation regions, without considering the too small BEMF [13]. Nevertheless, ADM generally has low saliency and even negative saliency, HF signal injection method is not applicable. For automotive ADMs' zero- and low-speed conditions, the current-frequency (*I–F*) sensorless method is not only simpler than the HF signal injection method, but also can effectively solve the with-load starting problem with high reliability [14]. In fact, the rotor position estimation performance for medium- and high-speed conditions in ADMs is more significant, so the extended back electromotive force (EEMF) based rotor position estimation with simple control algorithm is a promising solution.

The power steering motor in the electro-hydraulic oil pump assembly is exposed to extreme operating conditions with sudden load changes and is occasionally subjected to external perturbations, which poses a great challenge to the transient response characteristics of the motor. To solve this problem, the study of disturbance observer (DOB) and extended state observer (ESO) has been well developed. DOB can enhance the robustness of speed control system by estimating the disturbance [15] and can also be used to estimate the rotor position by observing the EEMF [16], although the gain parameters of DOB are difficult to design. In [17], two ESOs are used to estimate

Manuscript received 19 July 2022; revised 1 November 2022; accepted 26 November 2022. Date of publication 8 December 2022; date of current version 14 February 2023. This work was supported by the Research Fund for the National Natural Science Foundation of China under Grant 51975049. Recommended for publication by Associate Editor R. Kennel. *(Corresponding author: Cheng Lin.)*

Yao Xu and Cheng Lin are with the School of Mechanical Engineering, Beijing Institute of Technology, Beijing 100081, China (e-mail: xuyao@bit.edu.cn; lincheng@bit.edu.cn).

Jilei Xing is with the State Key Laboratory of Automotive Safety and Energy, Tsinghua University, Beijing 100084, China (e-mail: xingjilei699@163.com).

Color versions of one or more figures in this article are available at https://doi.org/10.1109/TPEL.2022.3226694.

Digital Object Identifier 10.1109/TPEL.2022.3226694

[1]This paper is not an extension of a conference paper.

the BEMF with an adaptive bandwidth tuning scheme and a quadrature phase-locked loop (PLL), which not only ensures excellent speed tracking performance but also significantly reduces the transient-state rotor position estimation error. Even so, this method ignores the degradation of the steady-state position estimation accuracy due to parameter mismatch.

Recently, active disturbance rejection control (ADRC) has shown great research and application prospects, mainly because it does not depend on an accurate mathematical model of the system and can accurately estimate and suppress the total disturbance including external load torque changes and internal motor parameter mismatch [18]. In combination with a sliding mode observer (SMO), linear ADRC was used in [19] and [20] to replace the current and speed loops in the conventional PMSM field-oriented control (FOC) system, respectively, which was able to achieve a fast dynamic response of the reference current and reference speed with small tracking errors. An ESO of linear ADRC based on the PLL principle was designed in [21] with different speed feedback to obtain the best disturbance and measurement noise rejection effect, respectively. In [22], a fractional-order ESO instead of integer-order ESO was designed to obtain better speed response characteristics and high robustness to controller gain variations. A linear/nonlinear ADRC switching control strategy was proposed in [23] to significantly reduce the overshoot of the speed response, but with more complex algorithms.

The ADRC studies of [19], [20], [21], [22], [23] were based on known rotor position information, which means that these studies were not necessarily applicable to sensorless control. In [24], a linear ADRC with cascaded second-order ESO was established based on the position and speed information obtained from the HF signal injection method, which was significantly more effective compared to the conventional single ESO method. However, the ADRC in [24] was only used for system disturbance estimation and does not work for estimating rotor position information. Besides, the cascaded ESO design requires more parameters to be tuned. Linear ADRC can be directly used to observe the BEMF [25] and EEMF [26] for rotor position estimation, respectively. With mitigation of adverse influence of the phase delay and chattering problems of SMO, the current regulation quality was dramatically enhanced.

In this article, a novel enhanced linear ADRC (ELADRC) sensorless control method based on EEMF observation is proposed. The transient-state response characteristics of the PMSM exposed to sudden load changes are improved without increasing the complexity of the algorithm. The novelty of this article lies in that the noisy rotor position signal estimated by the EEMF-based sensorless control method is utilized as the subject variable of ESO to obtain accurate rotor position information, thus avoiding the low-pass filter (LPF) and PLL design in the conventional EEMF-based method. Meanwhile, the adaptive mechanism of ESO is added to estimate the total system disturbance, which can improve the tracking characteristics and the suppression performance to the disturbance. The linear control law used to compensate the total disturbance can replace the speed loop PI controller in the FOC system, reducing the speed loop from a second-order system to a first-order system. The rest of this article is organized as follows: Section II presents the mathematical model and the problem analysis of the conventional position estimation method. In Sections III and IV, the design process and characterization of the proposed ELADRC are discussed. Section V shows the experimental results, which reveal the effectiveness of the proposed scheme on a 3kW automotive power steering oil pump motor drive system. Finally, Section VI concludes this article.

II. Sensorless Control Scheme Based on EEMF Estimation

A. Principle of the Rotor Position Estimation

The EEMF model of PMSM in a two-phase stationary α-β reference frame is expressed as follows [27]:

$$\begin{bmatrix} u_\alpha \\ u_\beta \end{bmatrix} = R_s \begin{bmatrix} i_\alpha \\ i_\beta \end{bmatrix} + \begin{bmatrix} sL_d & \omega_e(L_d - L_q) \\ -\omega_e(L_d - L_q) & sL_d \end{bmatrix} \begin{bmatrix} i_\alpha \\ i_\beta \end{bmatrix} + \begin{bmatrix} E_{ext,\alpha} \\ E_{ext,\beta} \end{bmatrix} \tag{1}$$

$$\begin{bmatrix} E_{\text{ext},\alpha} \\ E_{\text{ext},\beta} \end{bmatrix} = E_{\text{ext}} \begin{bmatrix} -\sin\theta_e \\ \cos\theta_e \end{bmatrix} \tag{2}$$

where u_α and u_β are the α- and β-axis stator voltages, respectively; i_α and $i_\beta$are the α- and β-axis stator currents, respectively; L_d and L_q are the d- and q-axis stator inductances, respectively; R_s is the stator resistance; ω_e is the rotor electrical angular speed, θ_e is rotor position, and s is the complex-frequency operator

$$E_{ext} = \omega_e\psi_f - s(L_d - L_q)i_q + \omega_e(L_d - L_q)i_d. \tag{3}$$

E_{ext}, expressed as (3), refers to the EEMF. i_d and i_q are the d- and q-axis stator currents, respectively; and $E_{\text{ext},\alpha}$ and $E_{\text{ext},\beta}$ are the EEMF components in α- and β-axis; and ψ_f is the permanent magnet flux linkage.

$E_{\text{ext},\alpha}$ and $E_{\text{ext},\beta}$ contain the rotor position information clearly, and stator voltages in (1) can be obtained from the reference voltages in the FOC with dead-time voltage deviation correction, and stator currents in (1) can be obtained through resistance sampling method. Supposed that estimated rotor electrical angular speed $\hat{\omega}_e = \omega_e$, $\hat{\omega}_e$ can be used for calculation in (1). Therefore, a current observer in a two-phase stationary α–β reference frame can be constructed as follows:

$$\begin{bmatrix} \dot{\hat{i}}_\alpha \\ \dot{\hat{i}}_\beta \end{bmatrix} = \frac{1}{L_d} \begin{bmatrix} u_\alpha^* \\ u_\beta^* \end{bmatrix} - \frac{R_s}{L_d} \begin{bmatrix} \hat{i}_\alpha \\ \hat{i}_\beta \end{bmatrix} - \begin{bmatrix} 0 & \frac{\omega_e(L_d - L_q)}{L_d} \\ \frac{-\omega_e(L_d - L_q)}{L_d} & 0 \end{bmatrix} \begin{bmatrix} \hat{i}_\alpha \\ \hat{i}_\beta \end{bmatrix} - \frac{1}{L_d} \begin{bmatrix} \hat{E}_{\text{ext},\alpha} \\ \hat{E}_{\text{ext},\beta} \end{bmatrix} \tag{4}$$

where u_α^* and u_β^* are the corrected stator reference voltages through the dead-time voltage deviation correction method used in [28] of the previous research. And $\hat{i}_\alpha$ and $\hat{i}_\beta$ denote the observed values of α- and β-axis stator currents, respectively. Since the current in the two-phase stationary reference frame can be obtained by direct measurement, then the observation error, which depends only on the value of the EEMF to be estimated, of the current observer is available in real-time. A PI regulator can be used as an error compensator, which in turn forms the entire EEMF observer

$$\begin{bmatrix} \hat{E}_{\text{ext},\alpha} \\ \hat{E}_{\text{ext},\beta} \end{bmatrix} = \left(K_p + \frac{K_i}{s} \right) \begin{bmatrix} \hat{i}_\alpha - i_\alpha \\ \hat{i}_\beta - i_\beta \end{bmatrix}. \tag{5}$$

The stability of the observer can be ensured by reasonably designing the parameter values K_p and K_i of the error compensator.

In addition, the uncertainty of the motor parameters in the observer can be partially compensated by the correction effect of the error compensator, which brings high parameter robustness. It is worth noting that when the *d*- and *q*-axis inductances are equal for an interior PMSM, the EEMF is equal to the BEMF of the motor. Therefore, the above observer model will be greatly simplified and still generalized.

Under the premise of stable convergence of the current observer, $E_{\text{ext},\alpha}$ and $E_{\text{ext},\beta}$ can be obtained, and thus the estimated rotor position can be calculated directly using the arctan function

$$\hat{\theta}_{e,\text{atan}} = \arctan\left(-\frac{\hat{E}_{\text{ext},\alpha}}{\hat{E}_{\text{ext},\beta}} \right). \tag{6}$$

B. Problem of the EEMF-Based Sensorless Control

Due to the large bandwidth of the current observer, the estimated EEMF inevitably contains many noisy signals, resulting in large fluctuations in the estimated rotor position obtained by direct calculation of the arctan function. To solve this problem, a PLL observer with suitable bandwidth is often adopted to obtain more accurate motor rotor position and speed estimation information simultaneously. Meanwhile, LPFs are needed to eliminate the HF components and reduce the position estimation noise for ensuring transient-state performance [29], [30]. However, this will make the observed output signal phase lag and degrade the steady-state performance of the PLL. The PLL and LPF approach cannot accurately track the rapidly changing speed, generating unavoidable transient-state position and speed estimation errors, especially when power steering motors face operating conditions with sudden load changes. Therefore, this processing of the preliminary estimated rotor position obtained from the EEMF observation cannot take both the steady-state and transient-state performance into account.

III. Design of Sensorless Control System Based on ELADRC Strategy

For the sake of improving the transient response characteristics of the automotive ADM, a sensorless control system based on the ADRC theory and EEMF rotor position estimation algorithm is proposed in this section in terms of both rotor position observation and speed loop controller.

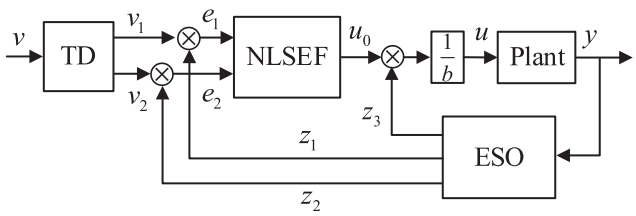

Fig. 1. Basic structure of ADRC.

A. Simplification of ADRC Structure

The ADRC system consists of four parts [31]: tracking-differentiator (TD); nonlinear state error feedback controller (NLSEF); ESO; and disturbance compensation, whose basic structure is shown in Fig. 1. Among them, the TD solves the contradiction between response speed and control overshoot in conventional PID control by designing a transition process for the step control reference command v; the ESO adds the internal and external disturbances of the system as an observation to the state equation, and uses the observation error to observe each state variable; and the NLSEF can generate the control signal u_0 of the control system based on the observation results of the ESO and be superimposed with the disturbance compensation z_3 to achieve highly robust control.

Considering that the automotive ADM needs high transient response capability only under rated operating conditions, its speed command is constant in this process, i.e., it does not need a TD for transition processing of the input speed command. In addition, the motor model parameters applied for different vehicles have the problem of frequent alterations and changes, therefore the nonlinear function has many coefficients that need to be tuned and calibrated. In view of this situation, the ESO and the state error feedback controller are linearized to simplify the whole design process.

B. Design of the Enhanced ESO

Based on the EEMF-based rotor position estimation algorithm [14], an enhanced ESO is used to replace the PLL position observer, and the load torque of the motor is referred to as total disturbance. To improve the transient response of rotor position and speed estimation, the disturbance observed by the enhanced ESO and the characteristics of the higher order state equation play a crucial role. The designed ELADRC substitutes the speed PI controller in the conventional FOC, and the stator reference current can be obtained after the flux-weakening control algorithm from compensated electromagnetic torque. The overall control scheme is shown in Fig. 2.

The motion equation of the PMSM can be expressed as

$$T_e - T_L = \frac{J}{n_p} \frac{d\omega_e}{dt} \tag{7}$$

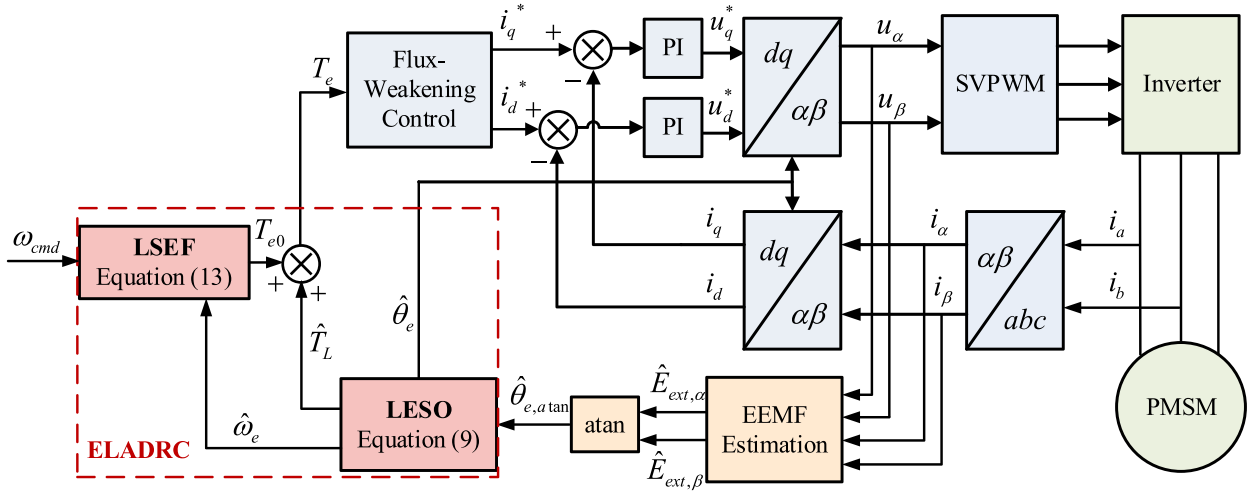

Fig. 2. Sensorless control scheme of ADM based on ELADRC theory.

where T_e and T_L are the electromagnetic torque and the load torque, respectively; and J and n_p represent the motor inertia and the number of pole pairs, respectively.

Specifically, select state variables $x_1 = \hat{\theta}_{e,a\tan}$ and $x_2 = \omega_e$, (7) can be transformed into the state equation as shown

$$\begin{cases} \dot{x}_1 = x_2 \\ \dot{x}_2 = x_3 + bu \\ \dot{x}_3 = \dot{d}(t) \end{cases} \tag{8}$$

where $b = n_p/J$ denotes the system input gain, $d(t) = -bT_L$ denotes the system total disturbance, $u = T_e$ is the system input, and the system output $y = x_1$. x_3 is the augmented state.

Based on (8), the enhanced linear ESO (LESO) can be designed by taking $\hat{\theta}_{e,a\tan}$ as the input subjective variable as follows:

$$\begin{cases} \varepsilon_1 = z_1 - x_1 \\ \dot{z}_1 = z_2 - \beta_1\varepsilon_1 - \beta_2\dot{\varepsilon}_1 \\ \dot{z}_2 = z_3 + bu - \beta_3\varepsilon_1 \\ \dot{z}_3 = -\beta_4\varepsilon_1 \end{cases} \tag{9}$$

where $z_1 = \hat{\theta}_e$ and $z_2 = \hat{\omega}_e$ are observed values of the system state variables; z_3 is the observed value of the system total disturbance $d(t)$, which is equal to observed load torque multiplied by the gain b, i.e., $z_3 = \hat{d}(t) = -b\hat{T}_L$; $\varepsilon_1 = \Delta\hat{\theta}_e$ is estimation error of rotor position. β_1, β_2, β_3, and β_4 represent the linear feedback gains.

In the conventional LESO described in [32], [33], $\hat{\theta}_e$ only relies on the integral of $\Delta\hat{\theta}_e$. The bandwidth used in this method must be set very large to maintain disturbance rejection ability, which introduces more noise into the system. Therefore, the observation accuracy reduces when the system is subjected to fast sudden load changes. While in the enhanced LESO, $\hat{\theta}_e$ is the sum of the proportional and integral terms of $\Delta\hat{\theta}_e$, which has both better dynamic characteristics and better observation accuracy.

The block diagram of the enhanced LESO system is shown in Fig. 3, and the system closed-loop transfer function is as follows:

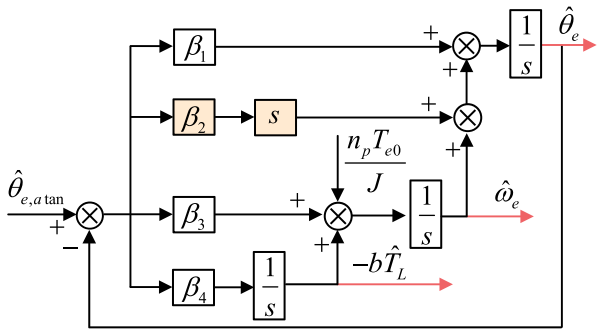

Fig. 3. Block diagram of the enhanced LESO.

$$\frac{\hat{\theta}_e(s)}{\hat{\theta}_{e,a\tan}(s)} = \frac{\beta_2 s^3 + \beta_1 s^2 + \beta_3 s + \beta_4}{(\beta_2+1)s^3 + \beta_1 s^2 + \beta_3 s + \beta_4}. \tag{10}$$

To ensure convergence of the enhanced LESO, all eigenvalues of the characteristic equation of the system composed of linear feedback gains should have negative real parts, so a simple gain design that satisfies this condition is

$$\begin{bmatrix} \beta_1 & \beta_2 & \beta_3 & \beta_4 \end{bmatrix}^T = \begin{bmatrix} 3r^2 & \omega_0 r^3 & -13r\omega_0^2 & \omega_0^3 \end{bmatrix}^T \tag{11}$$

where ω_0 and r are bandwidth and response factor of the enhanced LESO, respectively. Furthermore, based on the Routh criterion, the range of their values is determined as:

$$0 < \omega_0,\ 0 < r. \tag{12}$$

In fact, considering the boundary stability of the enhanced LESO and the practical results, it is recommended to limit the value r to $0 < r < 1$. It is worth noting that when $r = 1$, the designed enhanced LESO is the same as the conventional LESO.

C. Design of the Speed Controller

Among the observed values of the enhanced LESO, $\hat{\theta}_e$ will be used for Clark coordinate transformation in FOC control, $\hat{\omega}_e$ and its derivative will be used for speed loop control, $\hat{T}_L$ will

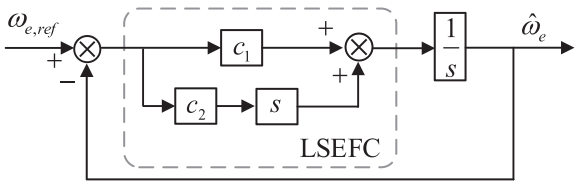

Fig. 4. Structure block diagram of speed loop based on LSEFC.

be used for disturbance compensation. Similarly, instead of the NLSEF, a linear state error feedback controller (LSEFC) is used

$$\begin{cases} e_1 = \omega_{e,\text{ref}} - \hat{\omega}_e, e_2 = \frac{d\omega_{e,\text{ref}}}{dt} - \frac{d\hat{\omega}_e}{dt} \\ T_{e0} = c_1 e_1 + c_2 e_2 \end{cases} \tag{13}$$

where $\omega_{e,\text{ref}}$ is reference speed, whose derivative is 0 at rated operating conditions; $\frac{d\hat{\omega}_e}{dt}$ must be derived from the enhanced LESO and cannot be obtained by taking the derivative directly concerning the estimated electrical angular speed; and c_1 and c_2 are the positive linear feedback gains.

With the assumption that the designed LESO can work normally in steady state, the observed values of the state variables can track the actual values with

$$\begin{cases} z_2 \to x_2 \\ z_3 \to x_3. \end{cases} \tag{14}$$

Therefore, with combination of control rate $u = (u_0 - z_3)/b$ of ADRC and state equation for $x_2$in (8), the following relationship can be obtained:

$$\dot{x}_2 = x_3 + bu = x_3 + b[(u_0 - z_3)/b] = u_0 \tag{15}$$

where u_0 is equal to T_{e0}.

Therefore, the speed loop can be considered as a unit gain integrator, which is controlled only by the linear state error feedback control law, as shown in Fig. 4.

In this case, the close-loop transfer function of speed loop can be obtained with combination and Laplace transform of (13) and (15) as follows:

$$G_{cl}(s) = \frac{x_2(s)}{\omega_{e,\text{ref}}(s)} = \frac{c_1}{(c_2+1)s + c_1} = \frac{1}{\frac{1}{\omega_c}s + 1} \tag{16}$$

where ω_c denotes the bandwidth of the speed loop, which determines the dynamic response capability of the system controller.

By comparison, if the speed loop PI controller is still adopted, the closed-loop transfer function of the speed loop in this case can be obtained in the same way as

$$G_{cl}(s)' = \frac{x_2(s)}{\omega_{e,ref}(s)} = \frac{k_p' s + k_i'}{s^2 + k_p' s + k_i'} \tag{17}$$

where k_p' and k_i' represent the control parameters of the PI controller.

Compared with the speed loop PI controller, the designed LSEFC can reduce the speed loop from a second-order system to a first-order system, which enables the DOB-based LSEF to achieve zero steady-state error without using an integrator. In addition, it avoids the more complicated parameter design and tuning work required by the PI controller to comprehensively consider the contradiction between the system response speed and the control overshoot.

Taking LESO and LSEFC into consideration, motor torque command can be obtained by superimposed disturbance compensation

$$T_e = T_{e0} + \hat{T}_L. \tag{18}$$

In fact, besides the load torque, there are also internal disturbances of the system, such as inaccurate motor inertia parameter, frictional drag, acceleration inertia forces, etc. The effects of these disturbances on the system will be included in the disturbance observation results together with the load torque, and thus do not affect the effectiveness of the ELADRC, which is the unique advantage of the ADRC, i.e., it is highly robust.

IV. Parametric Design and Characterization of the ELADRC

A. Stability Analysis

Considering that in the actual motor control system, the algorithm codes are executed in a digital signal processor (DSP) under discrete sampling conditions. Therefore, the designed enhanced LESO needs to satisfy the stability of the discrete system. According to the forward Eulerian discretization method [17], (8) can be transformed into

$$\begin{cases} x_1[k+1] = x_1[k] + T_s x_2[k] \\ x_2[k+1] = x_2[k] + T_s(x_3[k] + bu[k]) \\ x_3[k+1] = x_3[k] + T_s \dot{d}[k] \end{cases} \tag{19}$$

where k is the discrete sampling moment and T_s is the discrete sampling period. The enhanced LESO (9) can also be transformed into discrete forms according to the same approach

$$\begin{cases} \varepsilon_1[k] = z_1[k] - x_1[k] \\ z_1[k+1] = z_1[k] + T_s z_2[k] - T_s \beta_1 \varepsilon_1[k] \\ -\beta_2(\varepsilon_1[k+1] - \varepsilon_1[k]) \\ z_2[k+1] = z_2[k] + T_s(z_3[k] + bu[k]) - T_s \beta_3 \varepsilon_1[k] \\ z_3[k+1] = z_3[k] - T_s \beta_4 \varepsilon_1[k]. \end{cases} \tag{20}$$

Define $\varepsilon_i[k] = z_i[k] - x_i[k-1]$, where $i = 2, 3$. The following equation can be obtained from (20) minus (19):

$$\begin{bmatrix} \varepsilon_1[k+1] \\ \varepsilon_2[k+1] \\ \varepsilon_3[k+1] \end{bmatrix} = \underbrace{\begin{bmatrix} \frac{1-T_s\beta_1+\beta_2}{1+\beta_2} & \frac{T_s}{1+\beta_2} & 0 \\ -T_s\beta_3 & 1 & T_s \\ -T_s\beta_4 & 0 & 1 \end{bmatrix}}_{\mathbf{A}} \begin{bmatrix} \varepsilon_1[k] \\ \varepsilon_2[k] \\ \varepsilon_3[k] \end{bmatrix} + \begin{bmatrix} 0 \\ 0 \\ -T_s\dot{d}[k] \end{bmatrix}. \tag{21}$$

The sufficient condition for stability of (21) is to discriminate whether the eigenvalues of matrix **A** are within the unit circle of the z-plane. The characteristic equation of **A** can be calculated as shown

$$\Delta(z) = a_3 z^3 + a_2 z^2 + a_1 z + a_0 = 0 \tag{22}$$

where

$$\begin{cases} a_0 = T_s\beta_1 - \beta_2 - T_s^2\beta_3 + T_s^3\beta_4 - 1 \\ a_1 = T_s^2\beta_3 + 3\beta_2 - 2T_s\beta_1 + 3 \\ a_2 = T_s\beta_1 - 3\beta_2 - 3 \\ a_3 = 1 + \beta_2 \end{cases}. \tag{23}$$

Substituting (11) into (22), and based on the Jury criterion, the stability condition can be derived to the following set of inequalities:

$$\begin{cases} \Delta(-1) < 0 \\ |a_0| < a_3 \\ \left|a_0^2 - a_3^2\right| > |a_0 a_2 - a_1 a_3| \end{cases}. \tag{24}$$

Thus, the stable condition is obtained

$$0 < \omega_0 < \frac{2r}{T_s}. \tag{25}$$

B. Parameter Adaptive Design

According to (8) and (9), the error dynamics model of the designed LESO can be obtained as follows:

$$(1+\beta_2)\dddot{\varepsilon}_1 = -\beta_1\ddot{\varepsilon}_1 - \beta_3\dot{\varepsilon}_1 - \beta_4\varepsilon_1 - \dot{d}(t). \tag{26}$$

Therefore, the transfer function between $\varepsilon_1(s)$and $d(s)$ can be obtained as follows:

$$\frac{\varepsilon_1(s)}{d(s)} = \frac{-s}{(1+\beta_2)s^3 + \beta_1 s^2 + \beta_3 s + \beta_4} \tag{27}$$

where $d(s)$ is the Laplace transform of $d(t)$. After amplitude-frequency analysis, the relationship between the rotor position estimation error and the load torque disturbance to the system can be obtained

$$|\varepsilon_1(s)| = f(\omega, \omega_0, r)\,|d(s)| \tag{28}$$

with

$$f(\omega, \omega_0, r) = \frac{\omega}{\sqrt{\left[(\omega_0^3 - 3r^2\omega^2\omega_0)^2 + (3r\omega_0^2\omega - r^3\omega^3)^2\right.}}. \tag{29}$$

Obviously, if no other factors are considered, the rotor position estimation error is proportional to the load torque disturbance, which will significantly deteriorate the sensorless control performance. Therefore, some measures should be taken to ensure that the system still has good rotor position estimation performance when the load disturbance occurs. The ternary function $f(\omega, \omega_0, r)$ should remain negatively correlated with the absolute value of load torque disturbance $|d(s)|$ to ensure that $|\varepsilon_1(s)|$ is always less than a fixed threshold value at all working conditions.

On one hand, assuming that $r$and ω are fixed, $f(\omega, \omega_0, r)$ is monotonically decreasing in the interval of values of ω_0. On the other hand, assumed that $\omega_0$and ω are fixed, $f(\omega, \omega_0, r)$ is also monotonically decreasing in the interval of values of r. Fig. 5 shows simulation results of the rotor position estimation error variation versus r and ω_0 when the load torque disturbance is 60 N·m.

Therefore, based on simplification and practical experience, r and ω_0 are designed as a linear adaptive mechanism related to

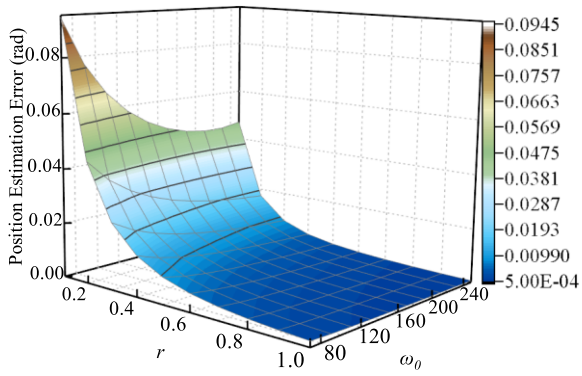

Fig. 5. Simulation results of the rotor position estimation error variation versus r and ω_0 when the load torque disturbance is 60 N·m.

$|d(s)|$ to suppress the effect of load torque disturbance on the accuracy of rotor position estimation

$$\begin{cases} r = a\,|d(s)| + b \\ \omega_0 = \omega'_0 + c\,|d(s)| \end{cases} \tag{30}$$

where a, b, and c are the adaptive factors of r and ω_0, which can be tuned through experiments; ω'_0 denotes the bandwidth of the conventional LESO. It should be noted that the actual disturbance is mutative under different operation conditions and is not directly available, so it can be approximated to the estimated load torque from the enhanced LESO.

C. Tracking Performance Analysis

Accurate and timely disturbance estimation is crucial to the tracking performance of the system. From (8) and (9), the transfer function between the estimated and actual disturbances in the frequency domain can be obtained as follows:

$$\begin{aligned} \frac{Z_3(s)}{X_3(s)} &= \frac{-\beta_4}{(1+\beta_2)s^3 + \beta_1 s^2 + \beta_3 s + \beta_4} \\ &= \frac{-\omega_0^3}{r^3 s^3 + 3r^2\omega_0 s^2 + 3r\omega_0^2 s + \omega_0^3}. \end{aligned} \tag{31}$$

For the conventional LESO without parameter adaptive mechanism, $r = 1$, and the bandwidth does not change with the load torque disturbance, which is set to $\omega_0 = 100$ for disturbance rejection. Therefore, the Bode diagrams of the disturbance closed-loop transfer function of the conventional LESO and enhanced LESO at different operating conditions are shown in Fig. 6. With the case where the load torque increases from 5 to 30 N·m in increments of 5 N·m, the tracking performance of conventional LESO and enhanced LESO remains unchanged as the blue dashed line shows and disturbance-varying as the solid line shows, respectively.

Since the load torque disturbance is often low-frequency, it is more necessary to focus on the tracking performance in the low-frequency range, where both conventional LESO and enhanced LESO perform well as shown in Fig. 6. However, the effective frequency range for conventional LESO is too narrow, which deteriorates the disturbance estimation accuracy. On the contrary, the enhanced LESO can perform better in the full

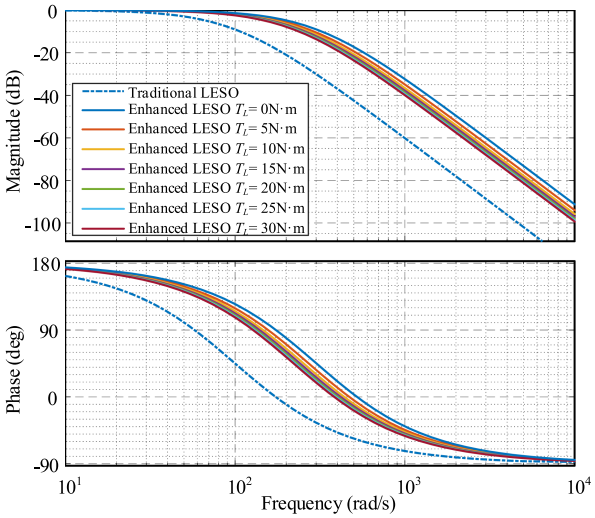

Fig. 6. Tracking performance of different methods.

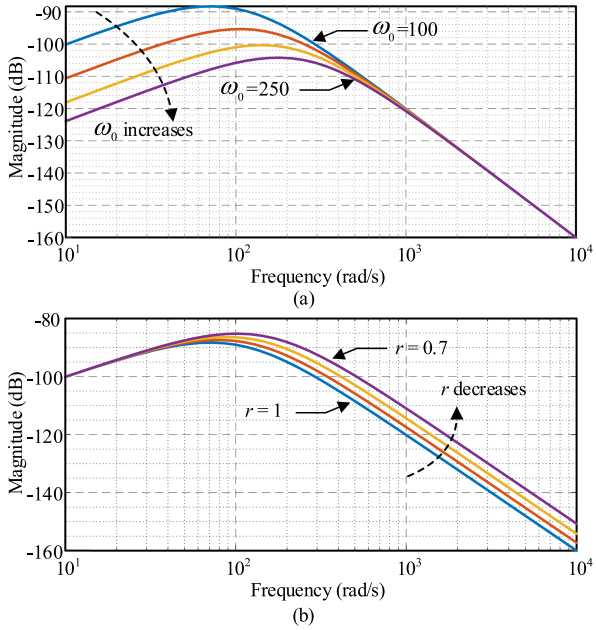

Fig. 7. Amplitude-frequency characteristic of (27). (a) $r = 1$, and ω_0 increases from 100 to 250 with an increment of 50. (b) $\omega_0 = 100$, and r decreases from 1 to 0.7 with a decrement of 0.1.

operating conditions and have a wider effective frequency range regardless of the variation of the actual load torque disturbance.

D. Influence of Nonideal Factors on the Proposed Strategy

Considering the influence of the saturation effect of the magnetic circuit, L_d and L_q are functions of the variations of i_d and i_q, and R and ψ_f are functions of the variations of motor temperature, which will affect the position estimation accuracy. Real-time variations in these parameters are captivating researchers for online parameter estimation of them for the high-performance control design of PMSMs [7], [34]. Most of these algorithms consume significant program execution time, and they may cause error propagation and deteriorate the performance of the controller when used in sensorless control. Although the proposed enhanced LESO is not influenced by the variations of these parameters, the real-time estimation by offline calibration and online look-up table method can ensure the effectiveness of the EEMF-based position estimation.

Nonsinusoidal magnetic flux distribution with higher order flux harmonics is inevitable in practical motor design and manufacturing process, which will specifically cause the sixth-order torque ripple[35]. Fig. 7 illustrates the amplitude-frequency characteristic of (27) for different values of ω_0 and r, which has a very low passband gain under a wide frequency range intuitively. And as ω_0 and r increase, the passband gain of the enhanced LESO gets lower, which demonstrates the strong disturbance rejection capability. Therefore, the 6th torque ripple at 600 Hz (3770 rad/s) is almost completely suppressed, not affecting the rotor position estimation accuracy.

V. Experimental Verification

The proposed transient response characteristics improvement of the position sensorless control based on ELADRC were verified on an experimental platform, which was established from the power steering oil pump assembly and the hydraulic circuit load to emulate the real vehicle load states. The parameters of the PMSM and the oil pump used are given in Table I. Fig. 8 shows the overall experimental system test bench and schematic diagram design. The inlet and outlet ports of the steering oil pump are connected to the oil storage tank through a hydraulic circuit, and the oil pressure at the outlet port can be quickly changed by adjusting the valve opening. An optical encoder is installed between the motor and the pump to test the estimation accuracy of the rotor position estimation and disturbance observation, and live experimental measurement results can be observed on the oscilloscope through signal conversion device for the optical encoder.

TABLE I
Parameters of PMSM and Oil Pump

Parameters (Units)	Value	Parameters (Units)	Value
Rated power (kW)	3	Pole pairs	4
Peak power (kW)	6	Stator resistance (Ω)	1.12
Rated torque (N·m)	23	d-axis inductance (mH)	12.52
Rated current (A)	10	q-axis inductance (mH)	23.37
Rated speed (r/min)	1500	Flux linkage (Wb)	0.263
Rated flow (L/min)	16	Relief valve pressure (MPa)	18

The motor controller used in the experimental verification is developed based on TMS320F28035 DSP with the main frequency of 60 MHz. The switching frequency of the controller IGBT power module is set to 6 kHz, which is consistent with the execution frequency of the motor FOC scheme and the

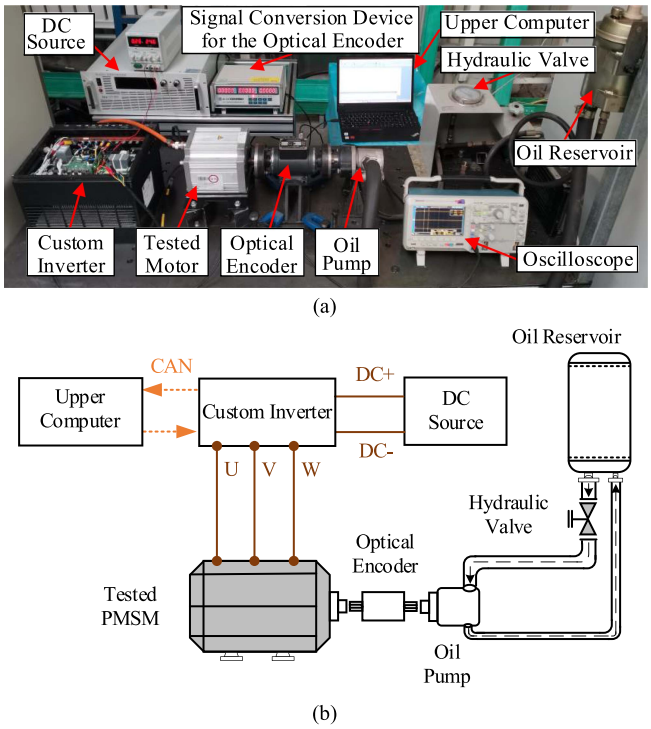

Fig. 8. (a) Overall experimental system test bench. (b) Schematic diagram design.

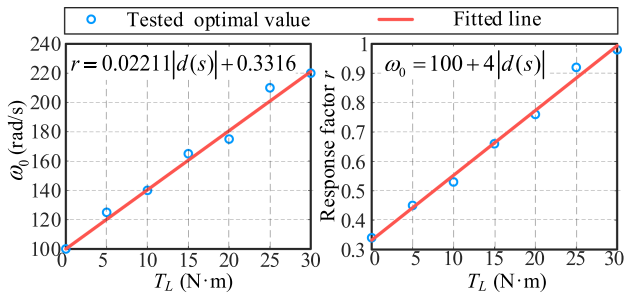

Fig. 9. Linear relationships of (30) fitted by the least squares linear fitting method.

sensorless control algorithm. The dc supply voltage is set to 550 V, and the upper computer is used to send commands to the controller and analyze estimated data via CAN communication.

The bandwidth of the speed loop is set approximately as $\omega_c = 95$ rad/s based on 1/20 of that of the current loop (300 Hz) according to a common rule of thumb[24]. Therefore, $c_1 = 96$ and $c_2 = 0.01$ are a set of suitable values based on experimental tests. The bandwidth of the conventional LESO is set to $\omega_0' = 100$ rad/s with a tradeoff between tracking performance and noise rejection performance. Taking the minimum speed fluctuation as the judgment criteria, the optimal values of r and ω_0 under each condition are obtained based on the experimental tests where the load torque step increases from 5 N·m to 30 N·m in increments of 5 N·m at rated speed. And the linear relationships of (30) with $a = 0.02211$, $b = 0.3316$, and $c = 4$ can be fitted by the least squares linear fitting method as shown in Fig. 9.

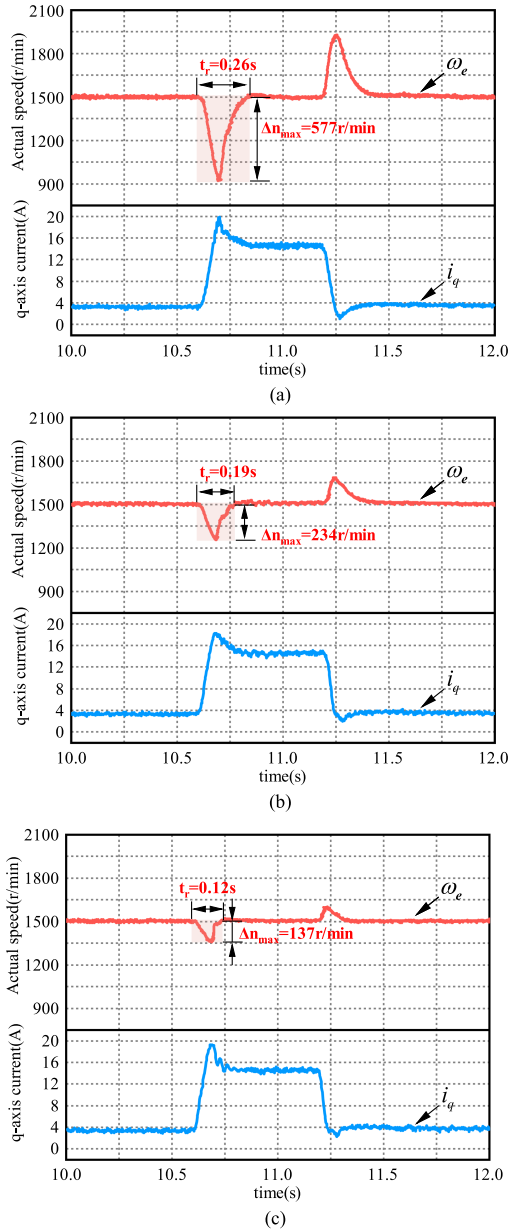

Fig. 10. Robustness comparison of different methods with a step peak-load torque under rated speed. (a) PLL observer with PI controller. (b) Conventional linear ADRC. (c) Enhanced linear ADRC.

A. Robustness Comparisons Between the Conventional Methods and the ELADRC

To verify the strong robustness of the proposed method compared with the conventional linear ADRC (CLADRC) based and PLL observer with PI speed controller-based EEMF sensorless control methods, the motor is subjected to load torque disturbance under rated speed. The adverse operating condition is the motor experiences a step peak-load torque change, i.e., the motor steps immediately to a peak torque of 44 N·m from the no-load state and then unloads.

Fig. 10 shows the dynamic speed response under the step peak-load torque change. During the sudden loading process, the motor dynamic response is more intense than that during the

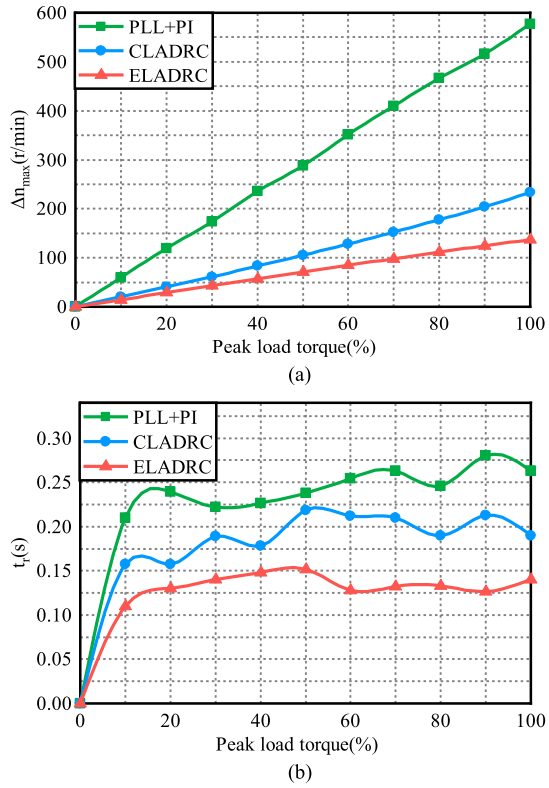

Fig. 11. Dynamic performance comparison of different methods at step load torque from 0% to 100% peak-load torque under rated speed. (a) Maximum speed fluctuation $\Delta n_{\max}$. (b) Speed recovery time t_r.

unloading process, so the analysis here will focus on the loading process.

The disturbance rejection impact can be judged by maximum speed fluctuation $\Delta n_{\max}$ and speed recovery time t_r. In general, the PLL observer with PI controller method has the worst performance in terms of speed dynamic response when disturbance occurs, and it can be inferred that there is even a risk of system instability if the system is under sustained step load disturbances. Although the CLADRC strategy performs better with $\Delta n_{\max}$ reduced to two-fifths, in contrast to the PLL observer with PI controller method, it is obvious that the system robustness to the disturbance is significantly improved by adopting the ELADRC strategy with the smallest $\Delta n_{\max} = 137$ r/min (9.13% of rated speed) and $t_r = 0.14$ s, which indicates clearly that the robustness of ELADRC strategy is superior to that of the other two methods.

In addition, for a more detailed and convincing comparison of the robustness of the conventional methods and the proposed ELADRC, other step load torque disturbance experiments are also implemented. The step load torque is changed from 0% to 100% peak-load torque with an increment of 10% of that at no-load conditions, and the speed dynamic response under different methods accordingly is shown in Fig. 11. It is worth noting that as the step load torque increases, the PMSM robustness to disturbance with the adoption of each method performs worse for $\Delta n_{\max}$ and t_r have an upward trend. Especially for the PLL observer with PI controller method, the speed fluctuation is much

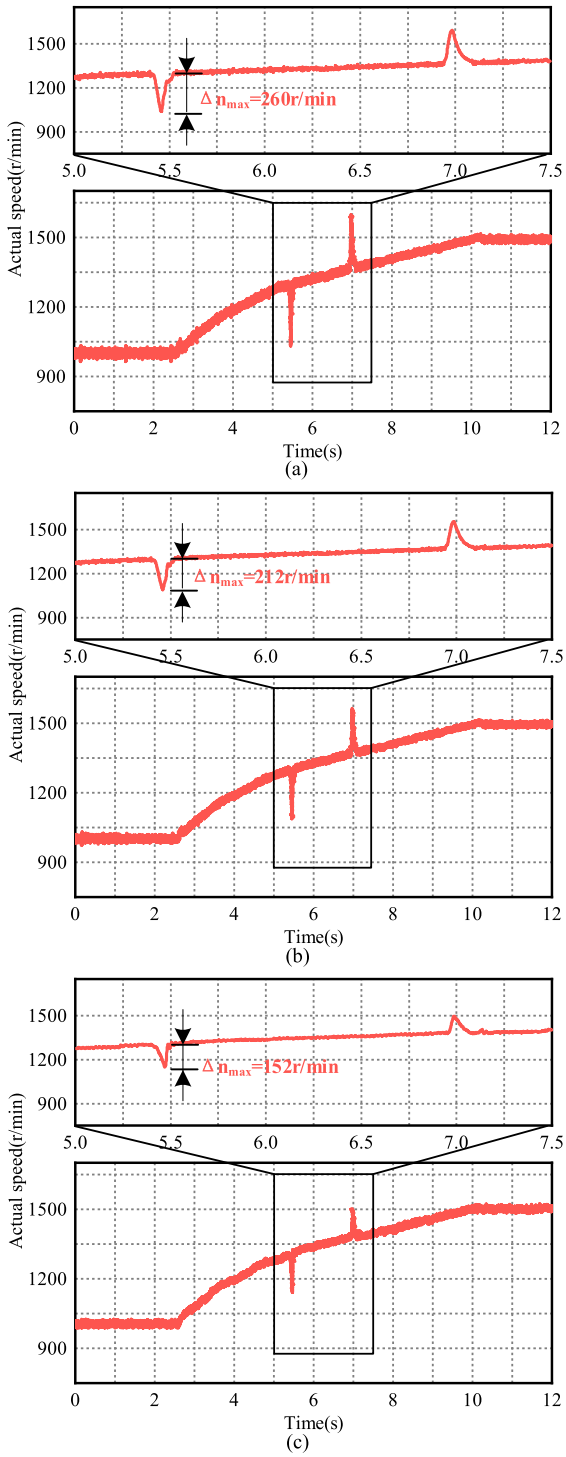

Fig. 12. Robustness comparison of different methods with a step peak-load torque under variable speed operation with speed rising from 1000 to 1500 r/min. (a) PLL observer with PI controller. (b) Conventional linear ADRC. (c) Enhanced linear ADRC.

larger than that of ADRC-based methods, which will pose a great challenge to the stability of the system control performance.

In order to further verify the generality of the proposed strategy, variable speed performance is very important for most PMSM drives. Additional experiments are carried out where

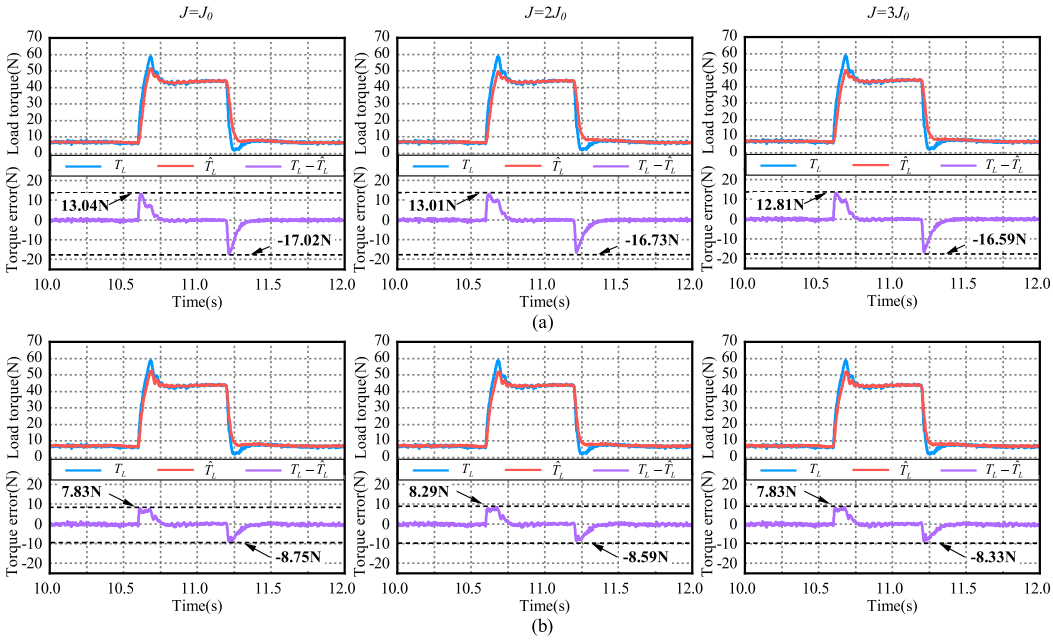

Fig. 13. Disturbance observation comparison when motor inertia varies. (a) Conventional linear ADRC. (b) Enhanced linear ADRC.

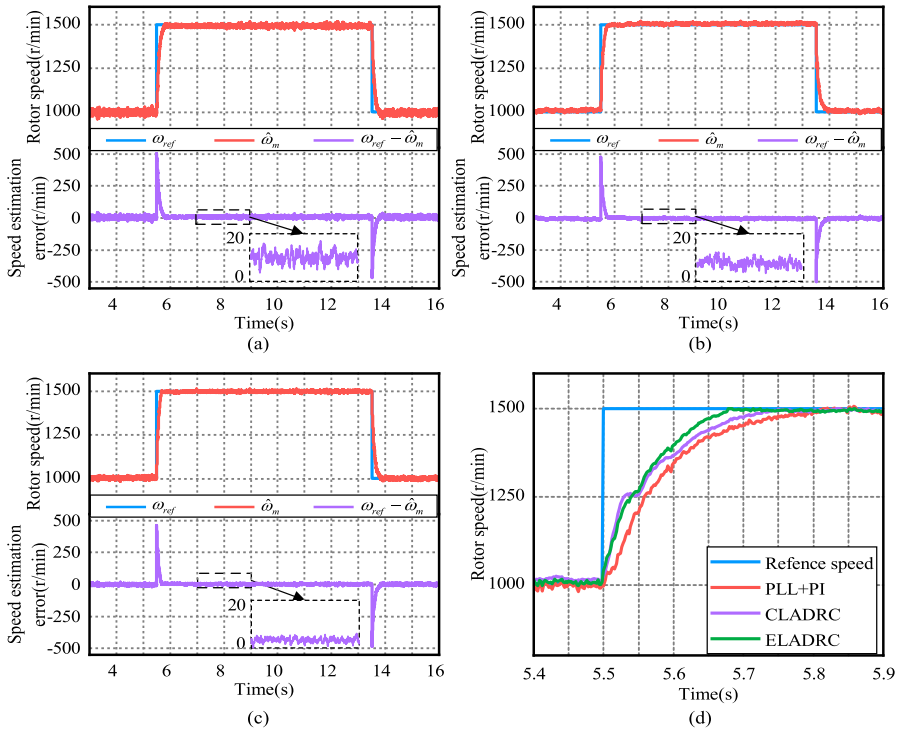

Fig. 14. Speed tracking performance under sudden reference speed changes. (a) PLL+PI. (b) Conventional linear ADRC. (c) Enhanced linear ADRC. (d) Comparison of transient responses of the three methods.

the motor is subjected to step peak-load torque change during the speed rise from 1000 to 1500 r/min. The robustness performances of the three different methods of PLL+PI, CLADRC, and ELADRC are shown in Fig. 12. It can be seen that ELADRC can still pass the test with step peak-load torque change under this extreme condition, and the speed fluctuation is only 152 r/min, which is significantly less than the 260 r/min of PLL+PI and 212 r/min of CLADRC. Meanwhile, ELADRC also has an advantage in terms of speed recovery time.

Furthermore, it is validated once again that the robustness performance of ELADRC is significantly superior to the conventional methods in the whole step load torque range with the smallest speed discrepancy both at rated speed and under variable speed conditions.

B. Tracking Performance Comparisons Between the ELADRC and the CLADRC

The ADRC design process brings a new parameter, i.e., motor inertia into the LESO structure. There is a high possibility that the motor inertia provided by the motor manufacturers have large errors or even not provided. Therefore, in order to validate the disturbance tracking performance of the proposed method, step peak-load torque change experiments are performed with different motor inertia under rated speed.

Fig. 13 shows the actual and estimated load torque when the motor inertia is set to the following three circumstances: $J = J_0$; $J = 2J_0$; and $J = 3J_0$, where J_0 is the actual inertia, with the employment of the CLADRC and ELADRC, respectively. On one hand, the motor inertia mismatch has a small effect on the tracking performance of ADRC-based sensorless control. The increased motor inertia only causes a very slight decrease in the convergence rate of the estimated load torque. On the other hand, with the same motor inertia, the disturbance tracking performance of ELADRC is superior to that of CLADRC for faster tracking speed and smaller estimation fluctuation during the step load torque process, which can be evaluated appropriately by the estimated error of load torque. By adopting the proposed ELADRC, the estimated error of load torque can be reduced almost to three-fifths under the loading process and almost to the half under unloading process, respectively. Generally, the motor inertia does not vary drastically like the electrical parameters with the change of motor operating conditions. Furthermore, the motor inertia error within a certain range can be calibrated by adjusting the feedback gain of the LESO, which reduces the impact on the control effect of ADRC.

The most common working condition of the oil pump motor is to work at the constant rated speed for more stable operation with higher efficiency, which only yields very little power losses compared with the mode of dynamically changing the motor speed to adjust the pump volume flow to the actual demand. In most other automotive applications, tracking fast changing desired speed references is a major issue, in particular for sensorless control. Experimental tests of the sudden change of the reference speed of the motor at the rated torque are elaborated below. The reference speed is stepped from 1000 to 1500 r/min, and then stepped down to 1000 r/min. Fig. 14(a)–(c) shows the reference speed, estimated speed and rotor speed error of the of PLL+PI, CLADRC, and ELADRC. The steady-state speed tracking errors of PLL+PI and CLADRC are 10 and 5 r/min, respectively, while that of ELADRC is 2 r/min, which shows its superiority in steady-state speed tracking performance. At the same time, during the instant of the reference speed step, the comparison of the transient speed changes of the three different methods is detailed in Fig. 14(d). ELADRC performs better than PI and CLADRC in transient speed tracking performance.

C. Position Estimation Comparisons Between the Conventional Methods and the ELADRC

Fig. 15(a)–(c) shows the position estimation error, actual and estimated position under step peak-load torque disturbance conditions of comparative experiments between the conventional methods and the ELADRC. Fig. 15(a) depicts the

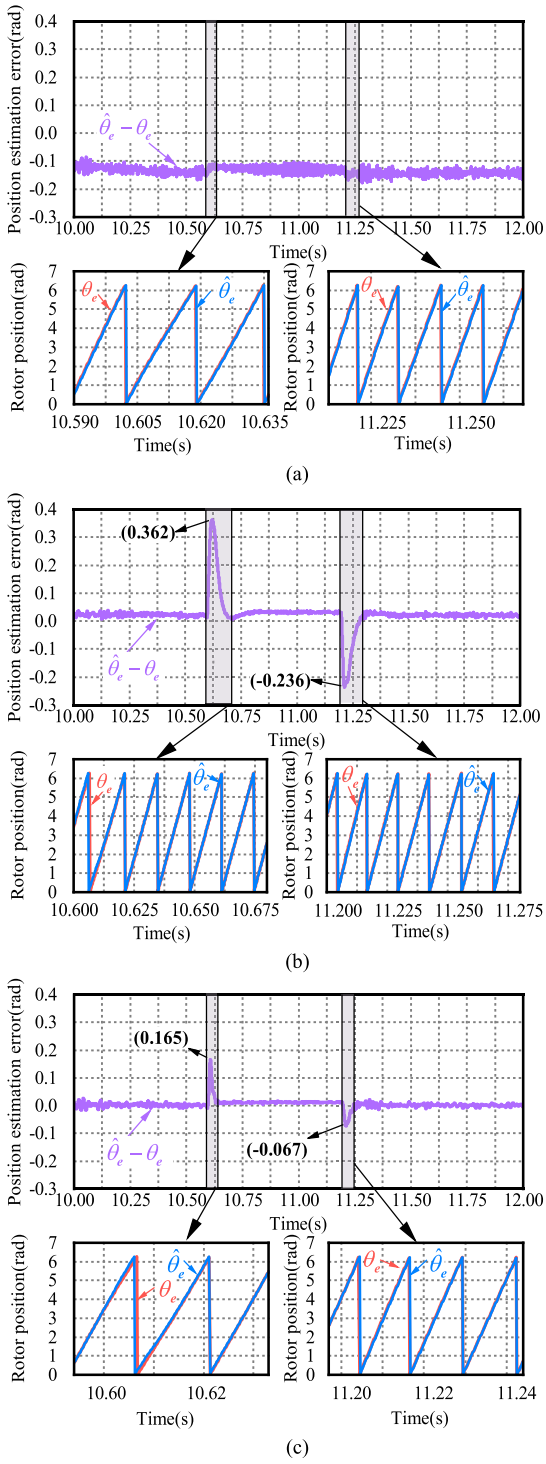

Fig. 15. Sensorless performance of different methods with step peak-load torque disturbance. (a) PLL observer with PI controller. (b) Conventional linear ADRC. (c) Enhanced linear ADRC.

average steady-state position estimation error of PLL observer with PI controller is about 0.137 rad and is not very sensitive to load torque disturbance. Antithetically, the average steady-state position estimation errors of CLADRC and ELADRC are much smaller as shown in Fig. 15(b) and (c), which are just 0.024 and 0.005 rad, respectively. It is worth stating that the estimation accuracy of ELADRC has been improved by 79.17% relative

to CLADRC. Evidently, the maximum position estimation error of CLADRC even reaches 0.362 rad in the presence of the step peak-load torque, which is prone to the problem of insufficient estimation accuracy and further reduced stability and dynamic performance. On the contrary, ELADRC does a good job of avoiding this situation, and its maximum position estimation error is just 0.165 rad ($<10°$). Applying a rule of thumb, the motor has tolerable control performance when the rotor position estimation error is within 10°. So, the dynamic rotor position estimation error of ELADRC in a small momentary interval can be neglected. Comprehensively, ELADRC possesses superior sensorless performance to that of conventional methods both under steady-state and transient-state conditions.

VI. Conclusion

This article proposed an ELADRC for improving transient response characteristics of PMSM used as ADM. The presented algorithm visibly enhances the speed robustness, disturbance tracking performance, and rotor position estimation accuracy during changes of motor load torque. The main conclusion is summarized as follows.

1) By adopting the novel LESO structure, the PMSM speed is more robust to the full range of load torque disturbance with a fast and low-oscillation recovery process of the smallest speed fluctuation within a shorter time.
2) It can be seen from both the theoretical analysis and experimental results that the ELADRC-based sensorless PMSM exhibits better tracking performance with accurate and timely disturbance estimation under various operating conditions of motor inertia, compared with the CLADRC-based sensorless PMSM.
3) The adaptive mechanism of LESO bandwidth is designed to reduce the position estimation error of ELADRC, and its average steady-state position estimation error is only 0.005 rad, which improves the position estimation accuracy by 79.17% compared to CLADRC. Generally, the position estimation accuracy of ELADRC is relatively accurate with almost zero steady-state error and tolerable transient-state error during the whole loading process compared to the above conventional methods.

References

[1] F. Yang et al., "Complex coefficient active disturbance rejection controller for current harmonics suppression of IPMSM drives," *IEEE Trans. Power Electron.*, vol. 37, no. 9, pp. 10443–10454, Sep. 2022.

[2] T. Tarczewski, R. Szczepanski, K. Erwinski, X. Hu, and L. M. Grzesiak, "A novel sensitivity analysis to moment of inertia and load variations for PMSM drives," *IEEE Trans. Power Electron.*, vol. 37, no. 11, pp. 13299–13309, Nov. 2022.

[3] L. Li, G. Pei, J. Liu, P. Du, L. Pei, and C. Zhong, "2-DOF robust H∞ control for permanent magnet synchronous motor with disturbance observer," *IEEE Trans. Power Electron.*, vol. 36, no. 3, pp. 3462–3472, Mar. 2021.

[4] Z. Huang, C. Lin, and J. Xing, "A parameter-Independent optimal field-Weakening control strategy of IPMSM for electric vehicles over full speed range," *IEEE Trans. Power Electron.*, vol. 36, no. 4, pp. 4659–4671, Apr. 2021.

[5] A. A. Alfehaid, E. G. Strangas, and H. K. Khalil, "Speed control of permanent magnet synchronous motor with uncertain parameters and unknown disturbance," *IEEE Trans. Control Syst. Technol.*, vol. 29, no. 6, pp. 2639–2646, Nov. 2021.

[6] G. Wang, M. Valla, and J. Solsona, "Position sensorless permanent magnet synchronous machine drives-A review," *IEEE Trans. Ind. Electron.*, vol. 67, no. 7, pp. 5830–5842, Jul. 2020.

[7] J. Zhang, F. Peng, Y. Huang, Y. Yao, and Z. Zhu, "Online inductance identification using PWM current ripple for position sensorless drive of high-Speed surface-Mounted permanent magnet synchronous machines," *IEEE Trans. Ind. Electron.*, vol. 69, no. 12, pp. 12426–12436, Dec. 2022.

[8] D. Xiao et al., "Universal full-Speed sensorless control scheme for interior permanent magnet synchronous motors," *IEEE Trans. Power Electron.*, vol. 36, no. 4, pp. 4723–4737, Apr. 2021.

[9] Q. An, J. Zhang, Q. An, and A. Shamekov, "Quasi-Proportional-Resonant controller based adaptive position observer for sensorless control of PMSM drives under low carrier ratio," *IEEE Trans. Ind. Electron.*, vol. 67, no. 4, pp. 2564–2573, Apr. 2020.

[10] Y. Yu, Y. Shao, F. Chai, and M. Cui, "Static-Errorless position estimation for sensorless PMSM drives with enhanced robustness against the full-Frequency domain disturbance," *IEEE Trans. Power Electron.*, vol. 37, no. 5, pp. 5884–5897, May 2022.

[11] X. Luo, Q. Tang, A. Shen, and Q. Zhang, "PMSM sensorless control by injecting HF pulsating carrier signal into estimated fixed-Frequency rotating reference frame," *IEEE Trans. Ind. Electron.*, vol. 63, no. 4, pp. 2294–2303, Apr. 2016.

[12] G. Wang, D. Xiao, G. Zhang, C. Li, X. Zhang, and D. Xu, "Sensorless control scheme of IPMSMs using HF orthogonal square-Wave voltage injection into a stationary reference frame," *IEEE Trans. Power Electron.*, vol. 34, no. 3, pp. 2573–2584, Mar. 2019.

[13] X. Wu et al., "Hybrid position estimation strategy with a smooth transition for IPMSM sensorless drives in the wide speed range," *IEEE Trans. Power Electron.*, vol. 37, no. 7, pp. 7916–7927, Jul. 2022.

[14] J. Xing, Z. Qin, C. Lin, and X. Jiang, "Research on startup process for sensorless control of pmsms based on I-F method combined with an adaptive compensator," *IEEE Access*, vol. 8, pp. 70812–70821, 2020.

[15] A. Apte, V. A. Joshi, H. Mehta, and R. Walambe, "Disturbance-Observer-Based sensorless control of PMSM using integral State feedback controller," *IEEE Trans. Power Electron.*, vol. 35, no. 6, pp. 6082–6090, Jun. 2020.

[16] D. Lee and K. Akatsu, "The study on sensor fault detection and algorithm transition using adaptive threshold in position self-Sensing control for IPMSM," *IEEE Trans. Ind. Electron.*, vol. 68, no. 11, pp. 10459–10466, Nov. 2021.

[17] F. Jiang et al., "Robustness improvement of model-Based sensorless SPMSM drivers based on an adaptive extended state observer and an enhanced quadrature PLL," *IEEE Trans. Power Electron.*, vol. 36, no. 4, pp. 4802–4814, Apr. 2021.

[18] W. Chen, J. Yang, L. Guo, and S. Li, "Disturbance-Observer-Based control and related methods—An overview," *IEEE Trans. Ind. Electron.*, vol. 63, no. 2, pp. 1083–1095, Feb. 2016.

[19] L. Qu, W. Qiao, and L. Qu, "Active-Disturbance-Rejection-Based sliding-Mode current control for permanent-Magnet synchronous motors," *IEEE Trans. Power Electron.*, vol. 36, no. 1, pp. 751–760, Jan. 2021.

[20] L. Qu, W. Qiao, and L. Qu, "An extended-State-Observer-Based sliding-Mode speed control for permanent-Magnet synchronous motors," *IEEE J. Emerg. Sel. Top. Power Electron.*, vol. 9, no. 2, pp. 1605–1613, Apr. 2021.

[21] Y. Zuo, X. Zhu, L. Quan, C. Zhang, Y. Du, and Z. Xiang, "Active disturbance rejection controller for speed control of electrical drives using phase-Locking loop observer," *IEEE Trans. Ind. Electron.*, vol. 66, no. 3, pp. 1748–1759, Mar. 2019.

[22] P. Chen, Y. Luo, W. Zheng, Z. Gao, and Y. Chen, "Fractional order active disturbance rejection control with the idea of cascaded fractional order integrator equivalence," *ISA Trans*, vol. 114, pp. 359–369, 2021.

[23] Z. Hao et al., "Linear/nonlinear active disturbance rejection switching control for permanent magnet synchronous motors," *IEEE Trans. Power Electron.*, vol. 36, no. 8, pp. 9334–9347, Aug. 2021.

[24] G. Wang, R. Liu, N. Zhao, D. Ding, and D. Xu, "Enhanced linear ADRC strategy for HF pulse voltage signal injection-Based sensorless IPMSM drives," *IEEE Trans. Power Electron.*, vol. 34, no. 1, pp. 514–525, Jan. 2019.

[25] L. Qu, W. Qiao, and L. Qu, "An enhanced linear active disturbance rejection rotor position sensorless control for permanent magnet synchronous motors," *IEEE Trans. Power Electron.*, vol. 35, no. 6, pp. 6175–6184, Jun. 2020.

[26] B. Du, S. Wu, S. Han, and S. Cui, "Application of linear active disturbance rejection controller for sensorless control of internal permanent-Magnet synchronous motor," *IEEE Trans. Ind. Electron.*, vol. 63, no. 5, pp. 3019–3027, May 2016.

[27] Y. Zhao, Z. Zhang, W. Qiao, and L. Wu, "An extended flux model-Based rotor position estimator for sensorless control of salient-Pole permanent-Magnet synchronous machines," *IEEE Trans. Power Electron.*, vol. 30, no. 8, pp. 4412–4422, Aug. 2015.
[28] C. Lin, J. Xing, and X. Zhuang, "Dead-Time correction applied for extended flux-Based sensorless control of assisted PMSMs in electric vehicles," *Electronics*, vol. 10, no. 2, 2021, Art. no. 220.
[29] X. Song, J. Fang, B. Han, and S. Zheng, "Adaptive compensation method for high-Speed surface PMSM sensorless drives of EMF-Based position estimation error," *IEEE Trans. Power Electron.*, vol. 31, no. 2, pp. 1438–1449, Feb. 2016.
[30] G. Zhang, G. Wang, D. Xu, and N. Zhao, "ADALINE-Network-Based PLL for position sensorless interior permanent magnet synchronous motor drives," *IEEE Trans. Power Electron.*, vol. 31, no. 2, pp. 1450–1460, Feb. 2016.
[31] J. Han, "From PID to Active disturbance rejection control," *IEEE Trans. Ind. Electron.*, vol. 56, no. 3, pp. 900–906, Mar. 2009.
[32] T. Zhang, Z. Xu, J. Li, H. Zhang, and C. Gerada, "A third-order super-twisting extended state observer for dynamic performance enhancement of sensorless IPMSM drives," *IEEE Trans. Ind. Electron.*, vol. 67, no. 7, pp. 5948–5958, Jul. 2020.
[33] Z. Xu, T. Zhang, Y. Bao, H. Zhang, and C. Gerada, "A nonlinear extended state observer for rotor position and speed estimation for sensorless IPMSM drives," *IEEE Trans. Power Electron.*, vol. 35, no. 1, pp. 733–743, Jan. 2020.
[34] S. J. Underwood and I. Husain, "Online parameter estimation and adaptive control of permanent-Magnet synchronous machines," *IEEE Trans. Ind. Electron.*, vol. 57, no. 7, pp. 2435–2443, Jul. 2010.
[35] Y. Xu, B. Zheng, G. Wang, H. Yan, and J. Zou, "Current harmonic suppression in dual three-Phase permanent magnet synchronous machine with extended state observer," *IEEE Trans. Power Electron.*, vol. 35, no. 11, pp. 12166–12180, Nov. 2020.

Yao Xu (Student Member, IEEE) received the B.S. degree in vehicle engineering from China Agricultural University, Beijing, China, in 2019. He is currently working toward the Doctor of Science in mechanical engineering with the School of Mechanical Engineering, Beijing Institute of Technology, Beijing, China.

His main research interests include the position sensorless control and parameter identification of auxiliary drive PMSM for commercial vehicles and high-speed PMSM for air compressors used in fuel cell vehicles.

Cheng Lin received the B.S. and M.S. degrees in mechanical engineering from the Wuhan Institute of Technology, Wuhan, China, in 1990 and 1995, respectively, and the Ph.D. degree in mechanical engineering from the Beijing Institute of Technology, Beijing, China, in 2002.

From 2010 to 2011, he was a Senior Research Fellow sponsored by the Country China Scholarship Council in the University of Michigan, Ann Arbor, MI, USA. Since 1995, he has been a Lecturer with the Department of Vehicle Engineering, School of Mechanical Engineering, Beijing Institute of Technology. He is currently a Professor, the Ph.D. Tutor, and the Director of Research Center for Electric Vehicle in Beijing. He has conducted extensive research in the field of electric vehicle, vehicle dynamics, and optimization and lightweight of automotive body structure.

Jilei Xing received the B.S. degree in vehicle engineering and Ph.D. degree in mechanical engineering from the Beijing Institute of Technology, Beijing, China, in 2016 and 2022, respectively. He is currently working toward the Postdoctoral research in mechanical engineering with the State Key Laboratory of Automotive Safety and Energy, Tsinghua University, Beijing, China.

His main research interests include position sensorless control, state estimation and current regulation of PMSM.